11

Strengthening mechanisms in nanocrystalline metals

D.G. MORRIS, National Center for Metallurgical Research (CENIM-CSIC), Spain

Abstract: This chapter examines the strengthening achieved as crystalline metals have their grain sizes reduced from large values down to the nanoscale. The well-known Hall–Petch strengthening observed as grain size reduces from large values continues well into the nano-regime, with a saturation or loss of strengthening sometimes observed for grains smaller than several tens of nanometres. This so-called inverse Hall–Petch dependence is often a consequence of material imperfections. New deformation mechanisms can, however, operate for grains smaller than tens of nanometres. The importance of second-phase particles, solute additions and ordering in strengthening nanoscaled materials is discussed, as well as the strengthening achieved by twin boundaries. The strengthening mechanisms in the nanostructured materials fabricated by severe plastic deformation are also considered.

Key words: strengthening in nanomaterials, Hall–Petch strengthening, grain boundaries, particle strengthening, solute hardening.

11.1 Introduction

One of the most interesting features of nanocrystalline materials is the possibility of increasing their strength to very high levels, approaching even what can be regarded as the theoretical strength for crystalline materials. This chapter will examine the strengthening achieved as the grain size of crystalline metals is reduced from the macroscopic to the microscopic level (from millimetres to microns) and then further, towards the nanolevel.

For materials with large grains, the build-up of stress concentrations at grain boundaries as deformation takes place in one grain, followed by the initiation of deformation in the second grain, leads to steady strengthening as grain size refines. This process, described by the well-known Hall–Petch relationship, continues to grain sizes well towards the nano-regime. In some experimental studies, such Hall–Petch strengthening continues to grains of only a few nanometres in size, while in other studies a saturation or even loss of strengthening is observed for grains smaller than some tens of nanometres. This loss of hardening has been termed the inverse Hall–Petch dependence. The origin of this loss of strengthening is examined, and seen to be often a consequence of material imperfections. As grain size falls below several tens of nanometres, however, a variety of other deformation mechanisms can operate, leading to changes in strengthening. These different deformation mechanisms are considered here, and their effect on strength discussed.

Most of the basic studies of nanocrystalline strengthening consider single-phase, often single-element material. The role of second-phase particles in strengthening nanoscaled materials is considered, and shown to be of considerable interest, as indeed is the strengthening achieved by solute additions or by ordering of the matrix. A high density of twin boundaries, or many nanothickness twinned regions, can also lead to considerable improvements in strength, with the attractive possibility of retaining better ductility or toughness. Such more complex nanocrystalline materials have been little examined and deserve further research attention. Finally, the strengthening mechanisms operating in nanostructured materials fabricated by severe plastic deformation will be considered. Such materials contain a mixture of dislocations and tangles, low-angle boundaries, as well as the usual high-angle grain boundaries, with each contributing to the overall strength.

11.2 The deformation of polycrystals; the Hall–Petch model for strengthening; typical strength and hardness data

Reducing grain size has long been seen as one of the most important ways to increase strength, with increased yield strength (σ_y) related to grain size (d) by the Hall–Petch equation:

$$\sigma_y = \sigma_0 + k\, d^{-1/2} \qquad [11.1]$$

where σ_0 is a friction stress and k a constant. This model for strengthening is based on the concept of strain within one grain being blocked by a grain boundary, leading to a grain-size dependent dislocation pile-up and stress concentration that induces new slip systems to operate in the second grain.[1] A smaller grain size implies a proportionally smaller pile-up, with reduced stress concentrating factor, to activate the new source, considered to lie within the neighbouring grain. This dependence of strength on a reciprocal square root of grain size is well established for conventional metals and alloys, although a dependency ranging from reciprocal cube root to reciprocal two-thirds root has been reported. The extension of Hall–Petch strengthening to the nanoscale has been reviewed on several occasions.[2–5]

Figure 11.1 shows an example of the hardness–reciprocal square root of grain size representation for Fe, with this grain refinement generally achieved by milling powders.[6–13] The data are reasonably well grouped, showing two linear regions, for coarse grain sizes (above 100 nm) and for very fine grain sizes. Clearly the Hall–Petch representation of hardening may be extended from very coarse grains to these finest grains, about 5–6 nm in size. Within the nano-regime, however, the Hall–Petch slope k is reduced from that typical of coarse-grained materials.

Figure 11.2 shows the corresponding Hall–Petch representation for a wide range of Cu samples prepared by plastic straining,[14,15] milling or inert gas condensation techniques,[16–19] with most of the powder samples compacted to bulk material. An extremely wide range of strengthening behaviour is observed,

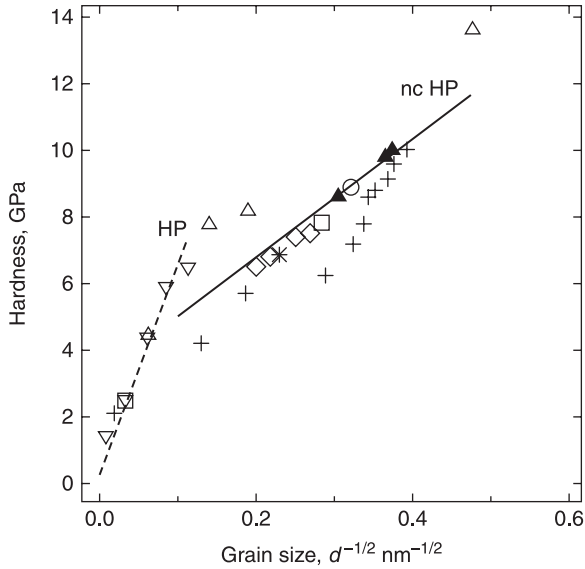

11.1 Variation of hardness of milled Fe related to the reciprocal square root of the grain size, i.e. a Hall–Petch representation. Source: Graph taken from Guduru *et al.*,[13] with source data indicated in the text.

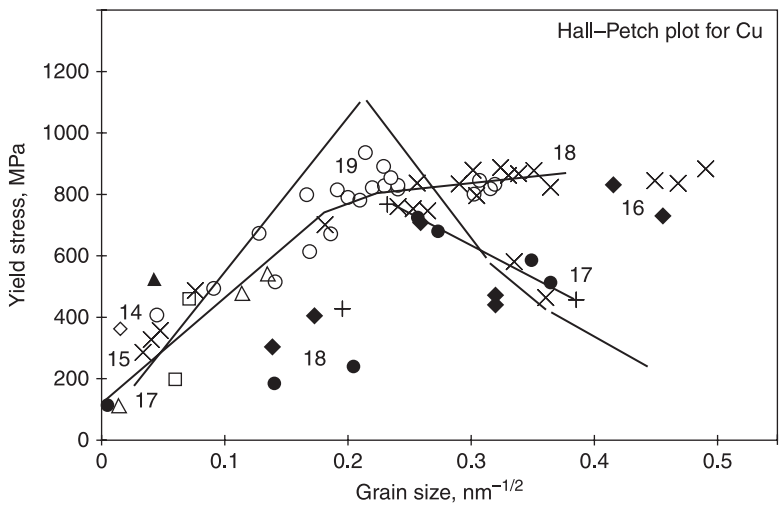

11.2 Variation of yield stress of Cu related to the reciprocal square root of the grain size. Sources of data[14–19] are indicated in the figure, which is adapted from Meyers *et al.*[4] Note that the lines shown are simply guides for the eye, illustrating the different families of strength variation observed during various studies by different researchers.

from a high value of Hall–Petch slope, similar to very coarse grains,[14,15] a very low value of Hall–Petch slope from coarse to fine grains,[16,18,20] a moderate Hall–Petch slope to some intermediate grain size followed by an absence of hardening,[19,21–24] or a moderate Hall–Petch slope to an intermediate grain size but followed by notable softening for finer grains.[17] Similar results have been obtained on a range of other nanocrystalline materials.[25–28] As will be discussed later in this chapter (Section 11.4) the unusual saturation of strength or softening found by some researchers at very fine grain sizes can generally be related to imperfections of material processing, for example retained porosity after powder compaction, leading to somewhat lower hardness and compressive strength and especially to reduced strength or premature failure when tested in tension.[18,19]

The Hall–Petch model has been many times criticised for relying on pile-up dislocation configurations, which are rarely observed in deformed materials, for producing stress concentrations near grain boundaries and for considering that the fresh Frank–Read type source lies within the new grain. Li[29] proposed instead that grain boundary ledges, on boundaries following deformation, acted as the sources for dislocations for propagation into the undeformed grain. This concept was subsequently modified by Ashby[30,31] who proposed that geometrically necessary dislocations were created near grain boundaries where the deforming grain interior evolved to the undeforming grain boundary region. Meyers and Ashworth[32] subsequently proposed a model, called the core-and-mantle model, which considered the polycrystalline material as a composite of hard grain boundary region with softer grain interior region. This model was based on the Ashby model of storage of geometrically necessary dislocations near grain boundaries, and also on the experimental observation of higher densities of stored dislocations near such boundaries and at triple points. This model was further extended by Benson *et al*.[33] to consider the nanoscale region where grain boundaries and triple points occupy a large fraction of the total volume. The low density of dislocations in grain interiors (core) allowed relatively easy dislocation glide and low work hardening, while the grain boundary regions (mantle) required extensive dislocation cutting and cross-slip such that both strength and work hardening rate were increased. The composite material strength (σ_C) could be described in terms of area fractions occupied by grain interior (A_G) and boundary regions (A_{GB}) and the strengths of these respective regions (σ_G and σ_{GB}) as:

$$\sigma_C = A_G\, \sigma_G + A_{GB}\, \sigma_{GB} \qquad [11.2]$$

The area fraction occupied by the hardened grain boundary region, including the triple point region, depends on the value of grain size relative to the thickness of the hardened region. Making various assumptions about the relation between thickness of the hardened region and grain size, a variation of composite strength with grain size (d) is deduced:

$$\sigma_C = \sigma_G + k_1\, (\sigma_{GB} - \sigma_G)\, d^{-1/2} - k_2\, (\sigma_{GB} - \sigma_G)\, d^{-1} \qquad [11.3]$$

From such ideas, we can understand that for large grain sizes (near the micron) the reciprocal square root term in equation 11.3 dominates, and the classical Hall–Petch dependence is observed. For very fine grain sizes, however, the reciprocal grain size term becomes dominant, and material strength will decrease. In an intermediate regime the apparent Hall–Petch slope will fall steadily, as strengthening evolves from classical Hall–Petch behaviour to strength saturation. Such saturation and eventual strength loss will occur at grain sizes similar in magnitude to the thickness of the grain boundary hardened region, which is presumably for grain sizes of several tens of nanometres.

In summary, strengthening as grain size is reduced can reasonably well be understood on the basis of classical dislocation theories, modified to take account of the large area of grain boundaries and their associated hardened regions as grain size falls to the nanolevel. A Hall–Petch dependency of yield strength (with reciprocal square root of grain size) is understood for coarse grain sizes in terms of the importance of hardened grain boundary regions where high dislocation densities accumulate during deformation. At grain sizes somewhere below 100 nm, the area fraction occupied by hardened grain boundary regions becomes large, with the thickness of this region a high fraction of grain size, and yield stress increases at a slower rate, eventually saturating at a strength maximum before falling.

11.3 Hall–Petch breakdown; a fine grain size limit to models

The Hall–Petch or Meyers–Ashworth models show that strength can be expected to increase proportionally with the reciprocal square root of grain size, and can be expected to be valid as long as the grains have sufficient space to retain the pile-up or hard-mantle/soft-core dislocation morphology. At very small grain sizes, however, there may be insufficient space to allow an array of more than 1–2 dislocations, which is hardly a pile-up, and equally there may not be space for the core and hardened morphology to be retained. Hence some fine grain size limit to the Hall–Petch type strengthening–grain size relationship may be expected.

At the same time, there are many observations of very low dislocation densities found in nanocrystalline materials after plastic deformation, and deformation is observed to localise into intense shear bands.[4,28,34,35] Deformation is typically associated with very low levels of work hardening, corresponding to the lack of an intense substructure forming during deformation. These observations appear inconsistent with the formation of pile-ups or intensely deformed grain-boundary regions. Such strain localisation into intense shear bands, and associated loss of work hardening capability, is already observed for grain sizes just below the micron (the transition from homogeneous to inhomogeneous deformation occurs in the 1000–100 nm grain size range), which is considerably above the grain size where the Hall–Petch relationship begins to fail, see Fig. 11.1 and 11.2. This would imply that the homogeneous–heterogeneous strain distribution has no

direct influence on the strengthening-grain size behaviour. Trelewicz and Schuh[28] disagree with this conclusion, however, since they observed homogeneous flow down to grain sizes of the order of 20 nm, just as the Hall–Petch relationship fails.

The grain size where strain concentration by dislocation arrays is no longer possible has been examined on several occasions. Nieh and Wadworth[36] considered the case where the elastic repulsion between the first and second dislocations of a nascent pile-up is greater than the material strength, since this implies that only single dislocations would be found in the given grain. This suggested a critical grain size (d_c), below which no pile-ups could form and hence Hall–Petch strengthening no longer be possible, given by:

$$d_c = G\, b/\{(1-\nu)\, H_v\}, \qquad [11.4]$$

where G is the shear modulus, b the Burgers vector, ν the Poisson's ratio and H_v the material hardness. Scattergood and Koch[37] and Koch[38] developed an analogous relationship by arguing that the Hall–Petch dependence would break down when the applied flow stress is sufficiently high to bow single dislocations, by a Frank–Read or Orowan type process, and the subsequent hardening-grain size relationship would be:

$$H_v = H_{v0} + k\,(1/2\pi\alpha_c).\{\ln(d/r_0)\}.d^{-1/2}, \qquad [11.5]$$

where H_v is the hardness of the material with grain size d, H_{v0} the hardness of single crystal material, k the Hall–Petch slope, α_c is $1/2\pi\ \{\ln(d_{crit}/r_0)\}$, with d_{crit} the critical grain size where Hall–Petch dependence no longer applies, and r_0 the dislocation core size. An alternative approach by Pande *et al.*[39] analyses the stress concentration at the pile-up tip in terms of the number of dislocation and the pile-up length, and shows that the Hall–Petch relationship can be respected down to pile-ups containing only about 2–3 dislocations, at which point the stress concentration becomes insufficient.

Examining these various expressions for limiting grain size[36–38] leads to the conclusion that the Hall–Petch relationship can be expected to be valid down to grain sizes of about 5–10 nm for Fe, 10–20 nm for Al and Cu, 10–15 nm for the ceramic TiO_2, with possibly larger values for materials such as some intermetallics with complex dislocation core structures. This conclusion is in general agreement with the data compiled in Fig. 11.1, showing that the Hall–Petch relationship is respected for Fe down to a grain size of at least 6–7 nm, but only in partial agreement with the Cu data of Fig. 11.2. In this figure, grains larger than about 20 nm generally show good grain-size hardening, while finer grains show great scatter and incompatibility of observed strength changes.

11.4 Hall–Petch breakdown: the importance of defective materials

The results presented in Fig. 11.1 and 11.2 and discussed above show that the strength–grain size dependence may be described by the Hall–Petch relationship

down to grain sizes of about 6 nm (for Fe; Fig. 11.1) or show highly variable behaviour for grains smaller than 50–100 nm (for Cu; Fig. 11.2). Classical dislocation theories suggest that such a relationship could well be valid down to grains sizes of approximately 5–20 nm. The next section will deal with other deformation mechanisms that may operate in materials with such very fine grain sizes, while the present section analyses the role of imperfections in the nanocrystalline state that appear to be responsible for the unusual and highly variable strength behaviour sometimes observed for grain sizes below about 100 nm. The term defective materials is used here to describe materials for which behaviour is dominated by processing inhomogeneities that are not, as such, intrinsic features of the nanocrystalline state.

This distinction between unusual and intrinsic nanocrystalline mechanical behaviour is particularly important in view of early ideas that grain boundaries in nanocrystalline materials were somehow special[40] and hence different behaviour might be possible from that expected of fine but normal material. Such early ideas suggested that grain boundaries in nanocrystalline materials had a lower atomic density than normal grain boundaries, with a more open atomic structure. Detailed studies of grain boundaries by High Resolution Electron Microscopy, however,[41] confirm that the atomic structure is very similar to that of equivalent boundaries in normal polycrystalline materials, with no evidence of any special structure.

Figure 11.3 shows three examples of results for Ni-base alloys where the Hall–Petch relationship is clearly not respected for grain sizes below 15 nm, 20–40 nm, and 120 nm, respectively.[5,28,42–43] In many such cases where behaviour different from the Hall–Petch relationship is found for relatively large grain sizes, simultaneous changes to microstructure or chemistry can be noted with changes to grain size. Thus, in the case of the electrodeposited Ni-Fe samples, Fig. 11.3 (a), the change of grain size is associated with a considerable change in Fe content.[42] Nanocrystalline materials prepared by electrodeposition, Fig. 11.3 (b),[28] often show major changes of chemical composition as grain size changes, with often poorly soluble metal or metalloid elements such as C, S or W present.[28,44–46] Such changes of composition, which may concentrate at grain boundary regions or be associated with changes of microstructure or texture[47] can, themselves, lead to significant changes of mechanical behaviour, thus making very uncertain the analysis of grain size dependence. The final example shown in Fig. 11.3 (c)[43] relates to an initially glassy Ni-P alloy, annealed to crystallise to different grain sizes. In this case there remains doubt about the possible retention of an amorphous layer between grains at grain boundaries for the finest grain sizes, and thus the true grain size dependence may be masked by other, dominating factors.

Many of the variable results found with regards to strength of nanocrystalline materials, especially those showing a low Hall–Petch slope, an apparent saturation of strength as the grain size refines, or an inverse Hall–Petch slope – all illustrated in Fig. 11.2 – were obtained by the study of inert-gas condensed powders which were subsequently compacted under vacuum by warm pressing.[16,22] These

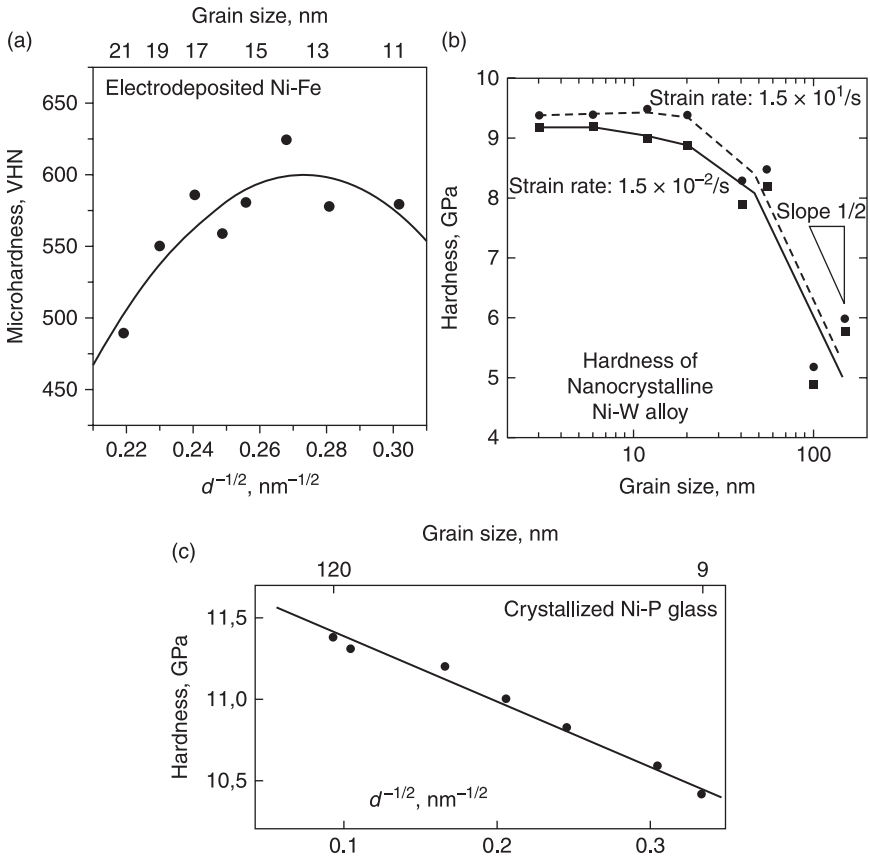

11.3 Variation of hardness with grain size for several nanocrystalline Ni-base samples, where anomalous, non-Hall–Petch dependence is observed for fine grain sizes. Sources: Data taken from (a) Cheung *et al.*;[42] (b) Trelewicz and Schuh;[28] and (c) Lu et al.[43]

materials are known to be highly flaw-sensitive[20,22,24,48] with considerable improvement in mechanical properties as the surface state of the mechanical testing samples is improved by better surface polishing,[18] or significantly higher strength when tested in compression (or by hardness) than when tested in tension.[19,24,26] The role of defects remaining after processing, especially the presence of retained porosity and gaseous impurities, is highly important in reducing strength and ductility, but also elastic modulus and other properties.[19,26] The retained gaseous content can be considerable, and will presumably lie at grain boundaries and cause significant changes in mechanical behaviour. As such, there is considerable doubt as to whether the observation of strengthening behaviour different from that expected from the Hall–Petch relationship (Fig. 11.2) is really due to the grain size variation, or is more likely associated with significant

amounts of retained porosity and gases, as well as changes in the perfection of grain–grain bonding.

Experiments comparing changes of strength as the nanocrystalline grain size is varied by different condensation–compaction conditions, or by annealing compacted materials, are worthy of especial attention.[21,49] Annealing a given sample to coarsen grain size can lead to strengthening – that is to an inverse Hall–Petch strength–grain size relationship. On the other hand, changing the evaporation–condensation–compaction conditions to obtain material with finer grain size also leads to increased hardness. The implication of these studies is that finer grain size, for equivalent grain boundary quality, and possibly different porosity and gas content, will lead to increased hardening; annealing alone will both coarsen grains and lead to improved bonding at boundaries and hence also strengthen these materials.

The important role of porosity, possibly imperfect grain boundary bonding, and retained gas content for this family of nanocrystalline materials is emphasised by noting the numerical values of such imperfections, and the progress in improving processing.[7,50] Despite optimisations of processing conditions, retained gas contents of ½–1 at.% each of hydrogen and oxygen are still found, with porosity levels as high as several percent. Such optimised materials are still likely to have mechanical properties significantly affected by imperfections. At the same time, it should be remembered that early samples (e.g. in 1990) prepared by such methods, contained significantly higher levels of imperfections, and such early strength–grain size behaviours should be treated with great caution.

As a final point, it should be remembered that this family of nanocrystalline materials will be expected to contain high densities of additional defects, for example stacking faults and high internal strain,[51] which may contribute to additional strengthening. Also, making this field subject to further uncertainty, it should be recalled that the clean nanocrystalline materials are highly unstable,[52] and may suffer changes of microstructure and grain size both during mechanical testing and during waiting periods (days, weeks) between material fabrication and testing.

11.5 Alternative deformation mechanisms at very fine grain sizes

It has been shown that it is possible to extend classical dislocation theories for hardening by grain boundaries down to grain sizes of the order of 5–30 nm, and thereafter it is uncertain whether such models are valid. There are nevertheless two other possible scenarios for changes of mechanism: 1) that well-known deformation mechanisms for coarse-grained materials may be activated by especially fine grain sizes and high boundary areas, or 2) that new mechanisms may appear at these very fine grain sizes and where very high stresses are required for conventional dislocation mechanisms. These will be the two aspects covered in the present section. First, we recall classical deformation mechanisms found in

normal polycrystalline materials that may be activated by very fine grain size, and then analyse the applicability of such mechanisms in various experimental studies. Secondly, we present several new mechanisms and again analyse their applicability to nanocrystalline materials.

11.5.1 Classical deformation mechanisms activated by fine grain sizes

Deformation mechanisms often found in conventional polycrystalline metals at somewhat elevated temperatures include diffusional creep and grain boundary sliding.[4,5,44] These may be activated at lower temperatures (i.e. room temperature) in materials with nanocrystalline grains since the deformation rate increases rapidly with decrease of grain size.

Two diffusional creep mechanisms may be considered, namely Nabarro–Herring creep,[53,54] equation 11.6, and Coble creep,[55] equation 11.7. The stronger grain size dependence exhibited by Coble creep means that this mechanism is more likely at nanograin sizes.

$$\dot{\varepsilon} = \frac{14\Omega\sigma D_l}{kTd^2}, \qquad [11.6]$$

$$\dot{\varepsilon} = \frac{14\pi\Omega\sigma\delta D_{gb}}{kTd^3}, \qquad [11.7]$$

where $\dot{\varepsilon}$ is the creep rate under the applied stress σ in material of grain size d, Ω is the atomic volume, k the Boltzmann constant, T the absolute temperature, D_l is the lattice diffusivity, D_{gb} the grain boundary diffusivity and δ the grain boundary thickness. These deformation mechanisms are characterised by a creep rate that increases linearly with applied stress and with reciprocal square (Nabarro–Herring) or reciprocal cube (Coble) of grain size.

Alternatively, sliding at grain boundaries may be the controlling deformation mechanism[56,57] with, again, lattice diffusion (equation 11.8) or grain boundary diffusion (equation 11.9) controlling stress relaxation at triple points, leading to creep rates of:

$$\dot{\varepsilon} = 8\times10^6 D_l\left(\frac{Gb}{kT}\right)\left(\frac{b}{d}\right)^2\left(\frac{\sigma}{G}\right)^2 \qquad [11.8]$$

$$\dot{\varepsilon} = 2\times10^5 D_{gb}\left(\frac{Gb}{kT}\right)\left(\frac{b}{d}\right)^3\left(\frac{\sigma}{G}\right)^2 \qquad [11.9]$$

In these equations, G is the shear modulus and b the Burgers vector, with other parameters having the same meaning as in equations 11.6 and 11.7. The creep rate now depends on the square of applied stress and again reciprocal square or

reciprocal cube of the grain size. An examination of the dependence of creep rate on applied stress and grain size, as well as an examination of the temperature dependence of creep rate, which will vary with the activation energies for lattice diffusion (Q_l) or grain boundary diffusion (Q_{gb}), thus allows the determination of the operating deformation mechanism.

11.5.2 Analysis of deformation of inert-gas condensed compacted-powder materials

Section 11.4 examined the saturation of or loss of strength observed in the inert gas condensed and compacted nanocrystalline materials at very fine grain sizes in terms of the possible importance of flaws remaining from imperfect fabrication. It is interesting to examine to what extent this strength saturation or loss may be caused by the onset of diffusional or sliding mechanisms requiring less applied stress than that expected by extrapolation of the Hall–Petch dependency.

The strength saturation or fall at the finest grain sizes has been observed on several occasions, and the possible onset of diffusional creep mechanisms suggested as a cause.[16,22] Chokshi *et al*.,[17] for example, analysed the softening found in Cu and Pd at grain sizes below about 15–20 nm in terms of the Coble creep mechanism, finding qualitative agreement. A later study of the temperature dependence of hardness of nanocrystalline copper by Huang *et al*.,[23] however, found a strong increase in hardness at low test temperatures that could not be explained by creep mechanisms. More detailed creep studies by Nieman *et al*.,[18,20] and by Sanders *et al*.[58] sometimes found linear creep,[20] that is, a steady increase in strain with time, but the creep rate measured was several orders of magnitude lower than expected for Coble creep, even without considering possible enhanced grain boundary diffusivity due to open grain boundary structures. Other studies[18,58] found that creep rates were not constant with time, as expected in diffusional creep and grain boundary sliding models, but instead decreased steadily. Creep rates dropping to much lower levels (several orders of magnitude) than expected in relation to the fastest Coble creep mechanisms have also been observed, possibly explained by grain boundaries having special orientations, or being low-angle boundaries where vacancy emission and absorption is much slower than for general boundaries.

In summary, the experimental data supporting the theory that diffusional or sliding creep mechanisms operate in these nanocrystalline materials at room temperature are inconclusive and unconvincing. Creep-like time-dependent deformation may indeed be observed on loading, but deformation rate may slowly decrease with time, as some exhaustion of the mechanism takes place, possibly related to the special nature of the grain boundaries and to some evolution with strain/time leading to more difficult vacancy emission or absorption.

11.5.3 Analysing deformation of other nanocrystalline materials

The results of some studies of creep-like deformation of nanocrystalline materials prepared by crystallization of metallic glasses and by electrodeposition are considered here to provide an overview picture of deformation mechanisms.

Studies of crystallised Ni-P and Fe-B-Si alloys[59–61] show much faster creep deformation for nanocrystalline grain sizes (27–28 nm) than for micron grain sizes. Analyses of the stress dependence and temperature dependence of creep rate appear generally consistent with the operation of Coble creep. Significant creep strain during a primary stage has been noted,[61] however, suggesting that other deformation mechanisms are also taking place. Absolute values of stress and temperature dependencies are nevertheless sometimes unusual, and it is clear that the deformation mechanisms occurring are more complicated and not completely understood.

Room temperature creep of electrodeposited nanocrystalline metals has been examined on several occasions,[44,62–64] considering the influence of grain size, applied stress and test temperature, typically slightly above room temperature. These are usually single-phase metals (e.g. Cu, Ni) containing small amounts of impurities necessary for obtaining the nanostructure. Grain sizes are typically about 6–50 nm. Wang *et al*.[44] examined the stress dependence of creep in nanocrystalline nickel with grain sizes of 6–40 nm, finding that the Hall–Petch relationship described strength down to grain sizes near 25–40 nm, but thereafter softening occurred. Grain boundary sliding was found for grain sizes of 20–40 nm, with dislocation creep becoming important when high stresses were applied. Much higher creep rates were found for material with 6 nm grain size, explained by diffusional creep, presumably Coble creep. The creep rate was not constant with time, however, and it again seems that the deformation processes taking place are more complicated than simply sliding or diffusional creep. Another study[64] of the creep behaviour of electrodeposited Ni with grain size of 30 nm again found significant primary creep before the onset of a steady-state regime that appeared to be controlled by Coble creep. Again in this study, a transition in deformation mechanism, to dislocation creep, was found at slightly higher temperatures. Creep deformation in nanocrystalline electrodeposited Cu with grain size of 30 nm has been examined on several occasions.[62,63] As observed for Ni, a significant primary creep stage was observed before a steady-state regime was established, where the creep rate varied linearly with applied stress, and the temperature sensitivity suggested a low activation energy, consistent with deformation controlled by Coble creep. More detailed investigation indicated, however, the existence of a strong internal stress (friction or back stress), only slightly lower than the applied stress. It was again suggested that the grain boundaries were imperfect sources or sinks for vacancies and many of these were low-angle or special/twin boundaries, a consequence of the electrodeposition process.

In summary, several studies have shown that Coble creep-like behaviour, or sometimes grain boundary sliding, may occur in nanocrystalline materials – based on the weak stress dependence of creep rate and low values of activation energy. It is, however, difficult to explain all aspects of this creep-like behaviour: notably a significant primary creep stage with the subsequent creep rate falling logarithmically and perhaps never becoming truly steady-state, and the detection of very significant internal or friction stresses opposing strain accumulation. It is still not completely certain whether the deformation observed is produced by diffusional/sliding creep mechanisms, whether such deformation is modified by the special nature of the grain boundaries present in nanocrystalline materials, or whether other, new deformation mechanisms are operating.

11.5.4 New experimental analysis of mechanical behaviour

Significant information for understanding deformation mechanisms in nanocrystalline materials has been obtained by analysis of deformation as a thermally activated process and the examination of parameters such as activation energy (ΔG or ΔF) and activation volume (ΔV). The present section examines these experimental analyses and the following section discusses the relevance for suggesting new deformation processes.

Treating deformation as a thermally activated process,[3,4,65] the strain rate $\dot{\gamma}$ can be written as:

$$\dot{\gamma} = \dot{\gamma}_0 \exp\left[\frac{-\Delta G(\tau^*_{\text{eff}})}{kT}\right] = \dot{\gamma}_0 \exp-\left[\frac{\Delta F - \tau^*_{\text{eff}}\Delta V^*}{kT}\right], \qquad [11.10]$$

where $\dot{\gamma}_0$ is a constant, $\Delta G(\tau^*_{\text{eff}})$ the Gibbs free energy of activation of the stress-dependent controlling process, k the Boltzmann constant, T the absolute temperature, ΔF the Helmholtz free energy (activation energy) and ΔV^* the effective activation volume. τ^*_{eff} is the effective shear stress, with $\tau^*_{\text{eff}} = \tau_{\text{appl}} - \tau_{\mu}$, and τ_{appl} the applied shear stress and τ_{μ} the athermal contribution to flow stress, i.e. long-range internal stresses opposing flow. Shear stress and strain may be related to applied stress and strain by $\tau = \sigma/\sqrt{3}$ and $\gamma = \sqrt{3}\,\varepsilon$, or $\dot{\gamma} = \sqrt{3}\,\dot{\varepsilon}$.

Activation energy can be determined by studying changes in strain rate as the temperature changes for the same effective stress. Activation volume can be determined from changes in strain rate as the effective stress changes, at constant temperature. There are two ways to achieve this, by jumping the strain rate, giving:

$$\Delta V = \frac{\sqrt{3}kT.ln(\dot{\varepsilon}_2/\dot{\varepsilon}_2)}{\Delta\sigma} \qquad [11.11]$$

where ΔV is the apparent activation volume and $\Delta\sigma$ the change in applied stress as the strain rate jumps from $\dot{\varepsilon}_1$ to $\dot{\varepsilon}_2$, or alternatively by examining stress changes during stress relaxation at constant total strain, giving:

$$\Delta\tau = \frac{kT.\ln(1+t/C)}{\Delta V}, \qquad [11.12]$$

where $\Delta\tau$ is the stress fall as a function of relaxation time t, and C a time constant. These two tests give an apparent activation volume which differs from the true activation volume (ΔV^*) as $\Delta V = \Omega.\Delta V^*$, where Ω is a factor depending on sample hardening during the tests and the test machine elasticity. The true activation volume can be determined by repeating stress relaxation tests, but such sophisticated tests are in fact rarely carried out. Such tests have suggested that the true activation volume is smaller than the apparent activation volume by a factor of about 2 to 3.[65]

The important point about analysing activation energy and volume is that these parameters are good indicators of the controlling deformation mechanism. It is rare that activation energies are measured[65] since achieving temperature changes without possible structural changes is difficult, but several measurements of activation volume have been reported.[2,3,65–67] Diffusional mechanisms, for example Nabarro–Herring and Coble creep, are characterised by activation volumes of about the atomic volume (or b,[3] where b is the Burgers vector). Similar values are presumably expected for grain boundary sliding. Dislocation movement (through a dislocation forest) in normal polycrystalline materials is characterised by activation volumes of the order of 1000 b^3 (where a long dislocation segment moves forward by a few Burgers vectors to cut through a forest dislocation). Studies of activation volume in nanocrystalline materials show intermediate values for ΔV, of the order of 10–100 b,[3] as illustrated in Figure 11.4, taken from

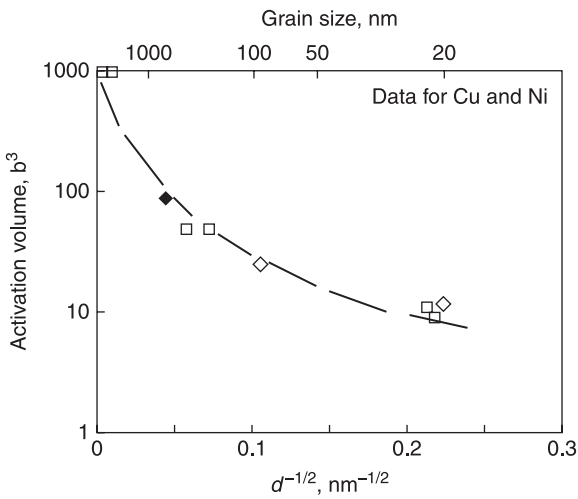

11.4 Values of activation volume measured in Cu and Ni for materials with a wide range of grain sizes, from the micron level down to the nanoscale. Source: Data taken from Dao *et al.*[3]

Dao *et al*.[3] This figure shows values of apparent activation volume measured in Cu and Ni as the grain size decreases from the micron level to about 20 nm. The activation volume decreases from about 1000 b,[3] typical of dislocation movement through a forest, to about 10 b^3 for the smallest grains. Similar values are reported for other nanocrystalline face-centred cubic (fcc) materials. Nanocrystalline body-centred cubic (bcc) metals show different behaviour since Peierls stresses play a significant role.[3,4] The small values of activation volume in the nanocrystalline fcc materials, derived from the large strain rate sensitivity, and seen also in a large temperature dependence of flow stress, indicate that neither conventional dislocation segments passing through dislocation forests nor diffusional creep processes control plastic deformation in these nanocrystalline metals. Measurements of activation energy are few: Wang *et al*.,[65] for example, determined a value of about 110 kJ/mol, corresponding to about $0.2Gb^3$ for nanocrystalline nickel, but it is difficult to find a clear explanation for this value.

11.5.5 Suggestions for new deformation mechanisms in nanocrystalline metals

Based on the analysis of strain rate sensitivity of flow stress, but also following insight gained from molecular dynamics modelling of such deformation, as well as detailed examinations of deformation by transmission electron microscopy, a new consensus of deformation mechanisms in nanocrystalline metals, with grain size significantly below 50 nm, is emerging.[3,4,65]

It has been known for a long time that work hardening is low in nanocrystalline metals,[5] which may be related to the very limited build-up of dislocation density and the absence of dislocation substructure during deformation. A more common observation is the nucleation of individual dislocations at grain boundaries, which then cross the grain, disappearing into the opposite grain boundary.[68–71] Examination of deformed materials by transmission electron microscopy is often frustrating since few dislocations remain. The dislocations emitted may be perfect dislocations for the given lattice, or imperfect dislocations that trail stacking faults or lead to twin development. This appearance of dislocations, and their subsequent disappearance, is also consistent with studies showing broadening of diffraction peaks during, but not after, deformation.[72] Other studies[73] show grain rotation occurring during deformation, presumably as dislocations move also within the grain boundaries.

Deformation controlled by the emission of such single dislocations is consistent with the small activation volumes determined, noting that this activation volume will be described as $\Delta = \beta.d.b.b$, where d is the grain size, b the Burgers vector, and β a factor of value 1/4–1/10 considering that the source emitting the dislocation segment is a small fraction of the grain size. Activation volume will fall as grain size reduces, to values of tens of b^3 for grain sizes of 20 nm, as in Fig. 11.4. There is thus good agreement between activation volumes and the model of single

dislocation emission.[2,3,65–67,74] This same model also implies that there is a tension–compression asymmetry of flow stress in nanocrystalline materials.[75]

Noting that the applied flow stress must supply an energy $1/2Gb^2.l$, where G is the shear modulus, b the Burgers vector and l the segment length (proportional to grain size) during creation of the new dislocation segment, it is clear that energy and stress requirements can be significantly reduced when partial, Shockley dislocations are instead emitted: energy is reduced to $1/6Gb^2.l$. This explains the activation of imperfect dislocation sources at very fine grain sizes, leading to stacking fault or twin appearance.[2,69–71,74] Such nucleation of partial dislocations will be easier in materials with low stacking fault energy (Ag, Cu) than in materials with high stacking fault energy (Al, Ni, Pd), but such deformation faults have indeed also been observed in deformed nanocrystalline Al and Ni. The appearance of such partial dislocations from the corresponding sources can be seen as a mechanism of softening, since such sources operate at stresses below that required for the equivalent perfect dislocation source.

Finally, we note that molecular dynamics simulation of deformation in nanocrystalline materials[76–78] is consistent with the experimental analyses in showing a transition from emission of perfect dislocations at grain boundary sources to partial dislocations at very fine grain sizes.[79,80] At the same time, atomic shuffling is seen inside the grain boundaries, somewhat similar to a grain boundary sliding or accommodation process. These simulations are consistent in showing easier deformation, at lower flow stresses, for grain sizes below about 10–15 nm.[81–83]

Thus, mechanical property analysis, transmission electron microscope investigation, and molecular dynamics simulation are essentially consistent in seeing an evolution of deformation mechanism as grain size reduces to very fine levels. For grain sizes above 50 nm, conventional dislocation behaviour can be expected, with stress concentrations and deformation propagation from one grain to another. For grain sizes of 20–50 nm, there is a transition to single dislocation emission from grain boundaries as the controlling process. In the grain size range 10–20 nm, the dislocations emitted change from being perfect dislocations to partial ones, with stacking faults and twin faults created by deformation. Below 10 nm, the role of grain boundary dislocations, atomic shuffles, and grain rotations becomes important, with stress falling to lower levels.

11.6 Strengthening caused by second-phase particles

Second-phase particles contribute to strengthening, as for conventional polycrystalline materials, where the particles are much finer than the grain size and distributed both within grains and at grain boundaries. For significant strengthening the particles must be relatively large, say 3–10 nm, and the simple discussion below considers that they are big enough not to be cut by dislocations, such that the Orowan mechanism operates. Such particles have sizes similar to the

grain size when this is fine, and in this case it is better to consider that the material is a composite mixture of matrix grains and particles.

Orowan hardening by fine particles, size ϕ, present in volume fraction f in a material of grain size $d >> \phi$, can be described as:

$$\sigma_{OR} = \frac{m2Gb}{1.18 \times 4\pi(\lambda - \phi)} \ln\left(\frac{\phi}{2b}\right), \quad [11.13]$$

where m is the Taylor factor, G the shear modulus, b the Burgers vector and λ the separation of particles on the shear plane.[84] The parameter λ is related to particle size as $\lambda = \phi/\sqrt{f}$. Since particles tend to pin grain boundaries, for materials in quasi-equilibrium after preparation by annealing (for powder consolidation, precipitation, coarsening, etc.) grain size and particle size are related, for example by the Zener relation, $d = 0.66\ \phi/f$, and hence grain size and particle separation are related:

$$d/\lambda = 0.66/\sqrt{f}. \quad [11.14]$$

As such, it is clear that Orowan strengthening models can only be used for materials containing a small volume fraction of second-phase particles, say less than 10%, and then the model applies independently of the grain size, nanoscale to microscale.

Figure 11.5 shows an analysis of strengthening in copper alloys containing second-phase particles,[84] where strength is related, via equation 11.13, through the Orowan mechanism. A good description of the particle strengthening, i.e. σ_{OR} proportional to $\{1/(\lambda - \phi).\ln(\phi/2b)\}$, is seen down to particle sizes of about 7 nm. Figure 11.6 shows some microstructures of these deformed particle-strengthened copper materials, where particle-dislocation interaction is clear. Since particle size can be related to grain size, equation 11.14, the strengthening may be re-expressed in terms of grain

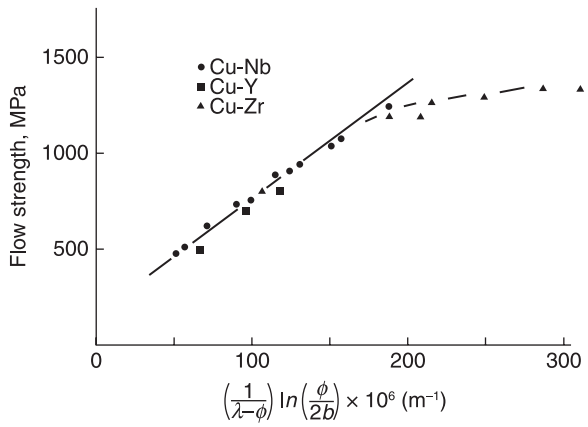

11.5 Analysis of strengthening in Cu-bcc particle materials in terms of the Orowan strengthening model, see text for details. Source: Morris and Morris.[84]

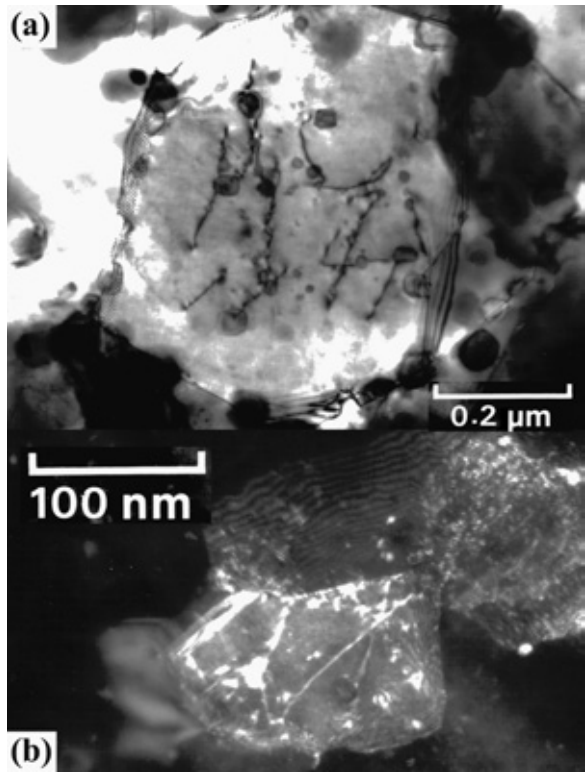

11.6 Transmission electron micrographs illustrating dislocation–particle interactions in Cu-bcc particle materials of fine grain size. Source: Morris and Morris.[84]

size, by the Hall–Petch equation (equation 11.1, $\sigma_y = \sigma_0 + k\, d^{-1/2}$) with relatively good agreement found. The numerical value of the Hall–Petch slope, k, is 0.28 MP$a\sqrt{m}$, however, much greater than the accepted values for a Cu matrix.[85,86] This analysis confirms that the major strengthening is due, in this case, to the particles present, and grain boundary strengthening is less important. A quantitative evaluation of Hall–Petch strengthening (equation 11.1) and Orowan hardening (equation 11.13), making use of the particle–grain size relation (equation 11.14) confirms that Orowan particle strengthening will dominate strengthening in Cu for particle sizes below about 20 nm and grain sizes below about 200 nm (for material with 5–10% second phase). The slower strengthening observed in Fig. 11.5 as the second-phase particles refine to very fine sizes (the near saturation in Fig. 11.5) may be due to particles shearing or to the loss of a homogeneous particle distribution with many particles trapped at the grain boundaries.

Another study examined hardening in nanocrystalline FeAl alloys and related strength to grain size[87,88] (Fig. 11.7), with data characterised by exactly the same

Hall–Petch slope as Fe (Fig. 11.1). These materials also contained fine Al_2O_3 particles, from oxidation during powder milling and during hot consolidation to solid material. The oxide particles are very fine here, less than 3 nm (see Fig. 11.8) and dislocations propagate with little effort since, presumably, they can shear the weak particles. Oxide particle coarsening on heat treating this material leads to initial strengthening, before softening through particle and grain coarsening – this evolution is indicated by the sequence of arrows in Fig. 11.7. More significant hardening has been produced in FeAl intermetallic by the addition of 30%TiC to the material, as indicated by the high-pressure data in Fig. 11.7.[89–91] These materials retained fine grain size, 20–30 nm, after high-temperature, high-pressure

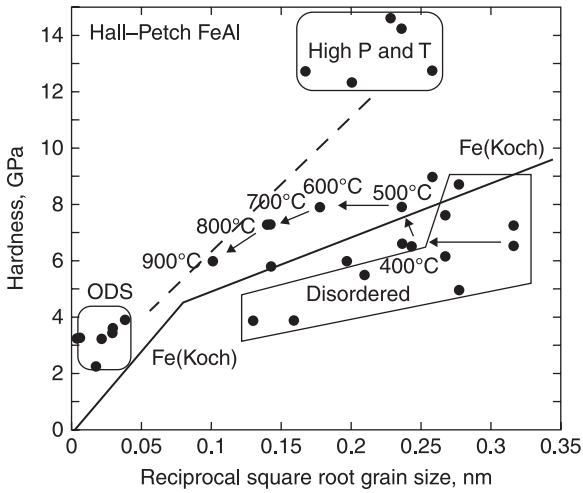

11.7 Hardness of several FeAl materials related to grain size by the Hall–Petch relationship. Data points connected by arrows indicate the hardness evolution on ageing, as oxide precipitates form.[88] Highest hardness is achieved after high pressure, high temperature consolidation of FeAl-TiC composites.[89–91]

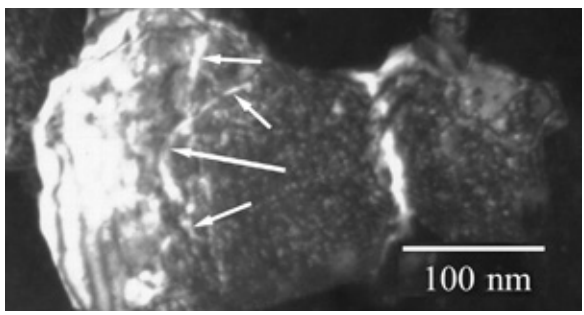

11.8 Transmission electron micrograph illustrating dislocation–particle interactions (arrowed) in FeAl.[88]

consolidation, but hardness can no longer be analysed by the Orowan model since both FeAl and TiC are of similar size and the material should be considered as a composite with mixed grains of the two phases.

When second-phase particles are present in large volume proportion (>10%) or the particles have a similar or larger size than the matrix grains, it is better to analyse material and hardness as a composite, where the rule of mixtures provides a good description (hardness is an area or volume-adjusted average of the hardness of the components). He and Ma[92] examined hardness in Cu-Fe composites, with an Fe content between 15 and 90%, and grain sizes of 25–45 nm for both phases, to find material hardnesses significantly greater than expected from the rule of mixtures, considering nanocrystalline Cu and nanocrystalline Fe. They concluded that the bcc–fcc interphase boundaries were much stronger than usual grain boundaries in either single phase Cu or single phase Fe. On the other hand, in studies on materials of Cu matrix and bcc second-phase additions,[93,94] the hardness observed for mixtures with Cu grain sizes between 10 and 60 nm fit well to the Hall–Petch relationship with a good value for the slope, k (0.16 MPa$\sqrt{}$m). In these cases, however, the volume fraction of bcc phase was small (5–10%) and bcc particles were somewhat larger than the Cu grain size, such that most boundaries present were standard fcc–fcc grain boundaries, and only few were bcc–fcc interphase boundaries.

Guduru *et al.*[13] also studied Fe mixed with Al_2O_3 and analysed hardness in terms of the rule of mixtures. This was justified since the Fe matrix grain size was about 10 nm but the Al_2O_3 particles about 50 nm. The experimental hardness was much greater than predicted by the rule of mixtures, see Fig. 11.9, and it was

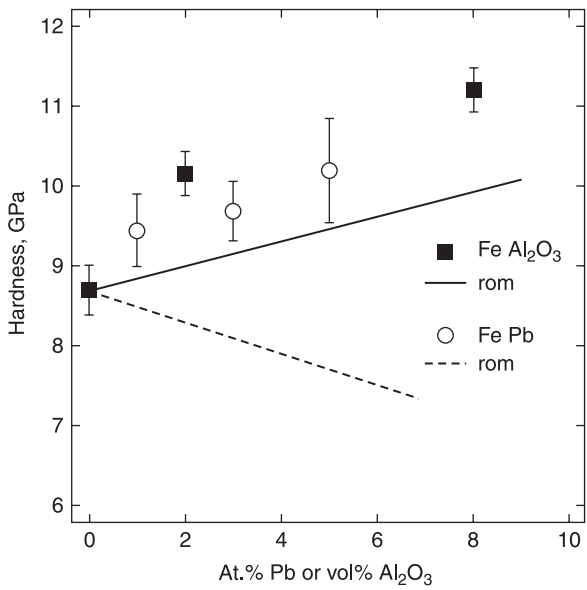

11.9 Hardness of Fe milled with Al_2O_3 and with Pb, indicating that the data do not fit to the composite rule of mixtures.[13]

argued that the much harder Al_2O_3 particles created a local heavily work-hardened zone in the neighbouring Fe grains due to the large number of geometrically necessary dislocations that formed there during deformation.

While most attention is given to strengthening by second-phase additions, and large second-phase particles seem generally associated with poorer ductility, there is some evidence that correctly sized and distributed second-phase particles might improve ductility. Dutta *et al*.[95] found that spherical second-phase particles of size slightly smaller than the matrix grain size, arranged on grain boundaries, might improve ductility by homogenising strain distribution during deformation.

Finally, reiterating Koch,[96] relatively little has been studied about the role of second-phase particles in affecting strength, toughness and ductility of nanocrystalline materials. There appears to be ample scope for improvement, and this area is one worthy of further investigation.

11.7 Strengthening caused by other factors: solute, order, twin boundaries

There are few studies that explicitly examine the role of solute or order of the nanocrystalline matrix in affecting mechanical behaviour. Guduru *et al*.[13] examined nanocrystalline Fe-Pb mixtures prepared by milling, using X-ray diffraction to confirm that the Pb had been dissolved. The disappearance, following milling, of diffraction peaks corresponding to Pb is insufficient, as such, to confirm Pb dissolution since X-ray diffraction is insensitive to the presence of small amounts of second phase present as fine particles. At the same time, however, the researchers observed a significant displacement of the matrix reflections, confirming the likely solution of up to about 5% Pb. Similar results on Pb dissolution during milling have also been observed by other researchers, see[13] for details. Fig. 11.9 shows the evolution of hardness with Pb addition, with a large increase with the 5% Pb addition. Hardness would be expected to fall if the Pb were present as second-phase particles, according to the composite rule of mixtures, indicated in Fig. 11.9. Examination of expected hardening by the large Pb atoms in the Fe matrix according to the Fleischer solution-hardening model showed, however, that even greater hardening should be expected. The authors speculated that the Pb atoms were not all uniformly distributed in solution and that some Pb could be present as segregation at grain boundaries or as sub-nanometric clusters, too small to be detected by standard diffraction methods.

Preparation of nanomaterials by milling techniques often leads to disordering of many intermetallics,[97,98] which can modify mechanical behaviour. For nanocrystalline FeAl, subsequent annealing at 150–250°C leads to re-ordering[87,88,98] but, as indicated in Fig. 11.7 by the arrows showing hardness evolution on annealing, there is no noticeable hardness change during this re-ordering.[88] One possible explanation is that the super-partial dislocation separation is so large for many such intermetallics that it is similar to the

nanocrystalline grain size and deformation is then accomplished by the partial dislocations that characterise the disordered matrix, somewhat analogous to the operation of partial dislocation sources (Shockley dislocations or twinning dislocations) suggested by molecular dynamics modelling.

Finally, while the theoretical models (Hall–Petch/Core-and-Mantle/Molecular Dynamics) do not clearly explain the role of solution additions on hardening, the evolution from a single perfect dislocation source to a single partial dislocation or twinning dislocation source, however, is clearly eased by alloying to lower stacking fault energy.

Improved strength is found also with finely spaced twins introduced by electrodeposition[99] or by rapid straining, especially at low temperatures[100–102] in materials with low stacking fault energy. Such twin strengthening can be found in grains of any size with the strengthening now determined by twin spacing instead of grain boundary spacing.[99] A significant advantage of nanospaced twin boundaries appears to be that ductility or toughness can remain high at the same time as strengthening is achieved.[101,103] Twins appear to act as barriers to dislocation slip operating in the parent grain, in much the same way as grain boundaries, requiring new slip activation in the twinned region or the parent-oriented region found behind the subsequent twin boundary.[104] Strengthening should then be described by the same formulation as for grain boundaries, such as the Hall–Petch approach. An alternative approach is to consider the twinned regions, which have nanoscale thickness determined by the close spacing of the pairs of bounding parent–twin interfaces, as hard regions of a composite, and then the overall material strength is given by a composite model of mixed hard and soft regions.[101] The low-energy, coherent twin boundaries appear, however, to be able to spread stress concentrations much more than occurs at grain boundaries, and hence are not the sites for crack or cavity nucleation as are grain boundaries or their triple points. This ability to suffer plastic deformation and store dislocations means also that the twin-strengthened materials possess some work hardening,[101,103] more than for nanoscale grain-boundary-strengthened materials, which is a second reason for the improved ductility of these materials.

11.8 Strengthening mechanisms in materials with ultrafine microstructure prepared by severe plastic deformation

Techniques of severe plastic deformation have been developed over the past about 20 years and shown to lead to microstructural refinement, towards the nanoscale, and to significant strengthening.[105,106] Techniques such as Equal-Channel Angular Pressing (ECAP) and High-Pressure Torsion (HPT) have been used to impose strains to of the order of (true strain) and above 100 for ECAP and HPT, respectively. Submicron or nanostructures can eventually be achieved at very high

strains in materials where recovery is slow or where multiple phase components impose strong microstructural refinement.

At the relatively low strains (2–8) generally achieved by the popular ECAP technique, however, the microstructure is composed of random dislocations within dislocation cell walls or low-angle grain boundaries (LAGB), contained within a smaller density of grain boundaries, or high-angle grain boundaries (HAGB). For example, deforming Al or Cu by ECAP to strains of 1–2 produces elongated dislocation cells; deforming to strains of 4 produces more equiaxed dislocation cell/subgrains; while deforming to strains of 10 produces microstructures of scale about 100–500 nm, where 50–70% of the boundaries have misorientations above 15°, i.e. are defined as HAGB.[105–107] Gubizca *et al*.[108] obtained similar dislocation cell structures in Al and Al-Mg alloy of size about 250–75 nm, respectively, after deforming to a strain of 2–8, where a dislocation density of $2 \times 10^{14} - 2 \times 10^{15}/m^2$, respectively, was measured. Similar structures are obtained in Fe and FeAl intermetallics,[109,110] where dislocation cellular structures are obtained after strains below 10, and nanocrystalline structures after strains above 100 imposed by HPT. After strains of about 3, the microstructure shows many randomly arranged dislocations inside a dislocation cell structure of size 200 nm with an average misorientation of 10° and 15% of boundaries being HAGB. A histogram of the distribution of boundary misorientations in this material, FeAl rolled to a strain near 3, is illustrated in Fig. 11.10.

Various explanations of strengthening during such severe plastic deformation have been proposed. Valiev *et al*.[109] argued that strengthening was caused by the many grain boundaries, i.e. by Hall–Petch strengthening, after heavy deformation

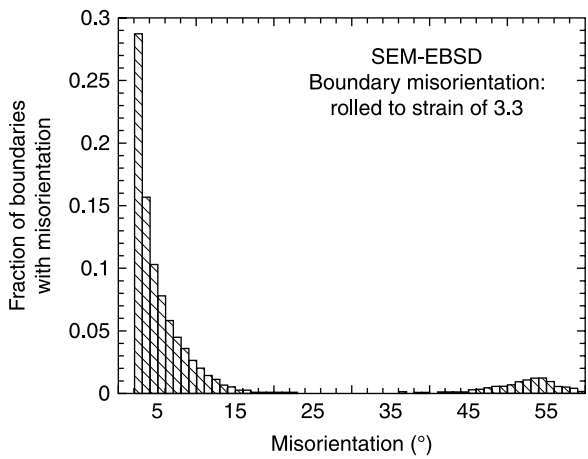

11.10 Histogram showing distribution of boundary misorientations in Fe_3Al rolled to a true strain of 3.3. Analysis by Electron Back-Scatter Diffraction in a Scanning Electron Microscope. Source: Adapted from Morris *et al*.[110]

to a nanocrystalline state. Gubizca *et al.*,[108] however, related strengthening ($\Delta\sigma_\rho$), through the Taylor equation, to the measured dislocation density (ρ_{loose}) as:

$$\Delta\sigma_\rho = M\alpha Gb\sqrt{\rho_{loose}} \quad [11.15]$$

where α is a factor of value about 0.3, M the Taylor factor, G the shear modulus, and b the Burgers vector. Leseur *et al.*[111] examined milled Fe and argued that a Hall–Petch dependence of hardening, i.e. $\Delta H \propto 1/\sqrt{d}$, could be expected for grain size d above 1 μm, but a subgrain size dependence, i.e. $\Delta H \propto 1/d$, for cells or subgrains smaller than 1 μm, i.e. about 50–1000 nm. In addition, they noted that hardening could be increased by nanosized oxide particles introduced during milling.

Hansen[85,86] has discussed how dislocation cell boundaries can be regarded essentially as additional dislocations, producing Taylor hardening, by converting cell boundary area and misorientation into equivalent dislocation density, ρ_{eff}. This approach seems reasonable but does not take complete account of the interaction of dislocation stress fields of closely spaced dislocations of different types, which will partially annihilate and reduce overall effectiveness as a barrier. With this approach, the strengthening from dislocation cell boundaries (LAGB) can be written:

$$\Delta\sigma_{cell} = M\alpha Gb\sqrt{\rho_{eff}} \quad [11.16]$$

with $\rho_{eff} = S_v\theta/b = 3\theta/d_c b$, and hence:

$$\Delta\sigma_{cell} = M\alpha G\sqrt{3\theta b/d_c} \quad [11.17]$$

where ρ_{eff} is the effective dislocation density inside cell walls, S_v the surface area of boundaries per volume, θ the boundary misorientation, and d_c the cell size. Note that equation 11.17 has the same dependency of strengthening on reciprocal square root of size as the Hall–Petch equation, with the effective Hall–Petch slope given by $k_{cell} = M\alpha G\sqrt{(3\theta b)}$. For small-cell boundary misorientations, the boundaries are much weaker than usual grain boundaries, but for misorientations reaching about 15° the value of k_{cell} is approximately that of $k_{H\text{-}P}$, justifying the common consideration that this misorientation marks the distinction between LAGB and HAGB.

Based on these arguments, the strength of a moderately deformed material should be seen as the sum of matrix friction stress σ_0, including any particle or solution terms, a loose dislocation term $\Delta\sigma_\rho$ taking account of dislocations inside cells, a dislocation cell term $\Delta\sigma_{cell}$, and a Hall–Petch term $\Delta\sigma_{HP}$ taking account of HAGB strengthening, thus:

$$\sigma = \sigma_0 + \Delta\sigma_\rho + \Delta\sigma_{cell} + \Delta\sigma_{HP} \quad [11.18]$$

An analysis of strengthening in heavily rolled Fe_3Al as strain level increases is shown in Fig. 11.11, where the dislocation hardening term $\Delta\sigma_\rho$ and the

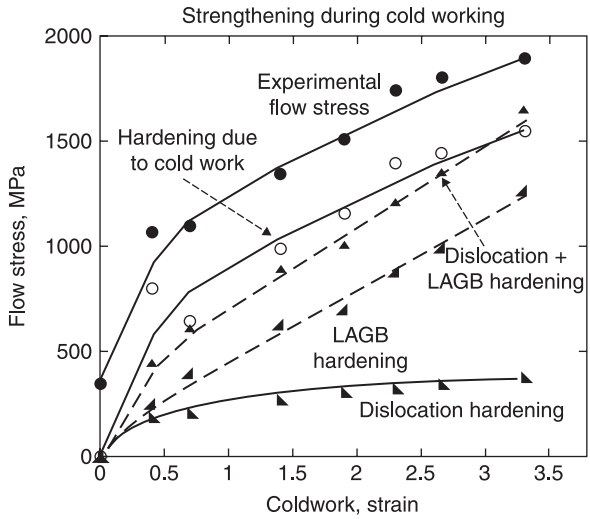

11.11 Analysis of hardening taking place during heavy rolling of Fe_3Al. Flow stress is interpreted as the sum of the initial, undeformed strength, an increase due to dislocation hardening, and hardening by cell boundaries (LAGB) created by deformation. Source: Taken from Morris *et al.*[110,112]

cell-LAGB hardening term $\Delta\sigma_{cell}$ are seen to add to the initial material strength ($\sigma_0 + \Delta\sigma_{HP}$) to provide a good description of the experimental strength.[110,112]

It can thus be understood that initial structural changes during deformation will cause rapid hardening as loose dislocations and dislocation cells are introduced, and only later will grain size hardening be significant as grain size is reduced significantly when LAGB (cell walls) slowly transition to HAGB (grain boundaries). Eventually, at nanoscale grain sizes, dislocation and cell hardening will be lost. A simple description of hardness as related to grain size (i.e. $\Delta H \propto 1/\sqrt{d}$) or as related to dislocation cell size (i.e. $\Delta H \propto 1/d_c$) will have some validity, each in its own given microstructural regime. Figure 11.12[109,110,112–115] compares hardening in Fe/Fe_3Al/FeAl during severe working, and shows how the $1/d$ dependence provides a better description of behaviour, with less data scatter, during the first stage of microstructure refinement, whilst the $1/\sqrt{d}$ dependence is better for grain sizes smaller than approximately 100 nm.

As a final comment, however, for grain sizes greater than about 50 nm, where a certain density of randomly arranged dislocation can be found (after deformation), and especially for grain sizes greater than about 100 nm, where dislocation cellular substructures are expected, the complete analysis of hardening must rely on equation 11.18, taking account of the density and misorientation of boundaries, as well as the presence of any loose dislocations.

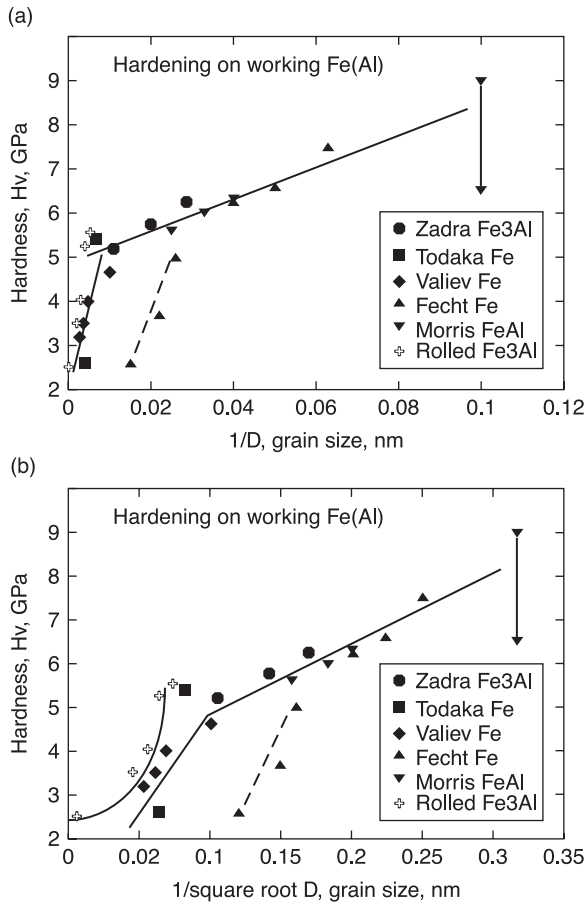

11.12 Analysis of hardening during cold working or milling of Fe/Fe_3Al/FeAl in terms of (a) reciprocal grain/cell size, or (b) reciprocal square root grain/cell size. Sources: Data taken from Valiev *et al.*;[109] Fecht *et al.*;[113] Todaka *et al.*;[114] Zadra *et al.*;[115] Morris *et al.*[110,112]

11.9 Conclusion and future trends

There now appears to be good understanding of the reasons for strengthening by grain size refinement, and especially the evolution from Hall–Petch behaviour, dependent on local stress concentrations in one grain inducing strain in neighbouring regions, to individual dislocation nucleation and glide, and eventually partial dislocation operation. Grain boundaries can be seen as both obstacles for dislocations and as sources, but the role of grain boundary sliding or diffusion, as well as the ideas of some special structure or behaviour of the boundaries, seems to be discredited.

Studies today concentrate on materials produced by new fabrication methods, including those prepared by severe plastic deformation and the nano-pillar class of samples, and on improving ductility or toughness at the same time as strength. The role of alloying to complex crystal structures and mixed-phase microstructures, which will surely improve both nanostructure stability as well as overall mechanical behaviour, remains poorly understood and worthy of further attention.

Specific references have been made throughout this chapter to important scientific publications. This is invaluable reading for a more profound understanding of this area. For the more general reader interested in a slightly deeper overview understanding of nanostructural strengthening than that presented here, the following reviews or general reports are recommended reading. Morris[5] gives a simple, now somewhat outdated overview of fabrication and mechanical behaviour of nanocrystalline metals. Meyers *et al*.[4] present a very complete analysis of strengthening in these materials. The importance of strain rate in analysing deformation is examined in some excellent publications by Asaro and Suresh,[2] Wang *et al*.[65] and Dao *et al*.[3] Finally, information on severe plastic deformation and its materials is reviewed by Valiev *et al*.[105] and Valiev and Langdon.[106]

11.10 References

1 Cottrell A.H. The mechanical properties of matter. McGraw-Hill, New York. 1964.
2 Asaro R.J., Suresh S. Acta mater 2005;53: 3369.
3 Dao M., Lu L., Asaro R.J., De Hosson J.T.M., Ma E. Acta mater 2007;55: 4041.
4 Meyers M.A., Mishra A., Benson D.J. Progress in mater sci 2006;51: 427.
5 Morris D.G. Mechanical behaviour of nanostructured materials. Trans Tech Publications. Uetikon-Zurich, Switzerland, 1998.
6 Jang J.S.C., Koch C.C. Scripta metall et mater 1990;24: 1599.
7 Fougere G.E., Weertman J.R., Siegel R.W. Nanostructured mater 1995;5: 127.
8 Zhu M., Fecht H-J. Nanostructured mater 1995;6: 921.
9 Rawers J.C., Korth G. Nanostructured mater 1996;7: 25.
10 Malow T.R., Koch C.C. Acta mater 1998;46: 6459.
11 Munitz A., Livne Z., Rawers J.C., Adams J.S., Fields R.J. Nanostructured mater 1999;11: 159.
12 Jia D, Ramesh KT, Ma E. Acta mater 2003;51: 3495.
13 Guduru R.K., Scattergood R.O., Koch C.C., Murty K.L., Guruswamy S., McCarter M.K. Scripta mater 2006;54: 1879.
14 Embury J.D., Keh A.S., Fisher R.M. Trans metall soc AIME 1966;236: 1252.
15 Hansen N., Ralph B. Acta metall 1982;30: 411.
16 Nieman G.W., Weertman J.R., Siegel R.W. Scripta metall 1989;23: 2013.
17 Chokshi A.H., Rosen A., Karch J., Gleiter H. Scripta metall 1989;23: 1679.
18 Nieman G.W., Weertman J.R., Siegel R.W. J mater res 1991;6: 1012.
19 Sanders P.G., Eastman J.A., Weertman J.R. Acta mater 1997;45: 4019.
20 Nieman G.W., Weertman J.R., Siegel R.W. Scripta metall et mater 1990;24: 145.
21 Fougere G.E., Weertman J.R., Siegel R.W. Nanostructured mater 1993;3: 379.
22 Gertsman V.Y., Hoffman M., Gleiter H., Birringer R. Acta metall et mater 1994;42: 3539.

23 Huang Z., Gu L.Y., Weertman, J.R. Scripta mater 1997;37: 1071.
24 Youngdahl C.J., Sanders P.G., Eastman J.A., Weertman J.R. Scripta mater 1997;37: 809.
25 Jain M., Christman T. Acta metall et mater 1994;42: 1901.
26 Hoffman M., Birringer R. Acta mater 1996;44: 2729.
27 Volpp T., Goring E., Kuschke W.M., Arzt E. Nanostructured mater 1997;8: 855.
28 Trelewicz J.R., Schuh C.A. Acta mater 2007;55: 5948.
29 Li J.C.M., Chou Y.T. Metall mater trans 1970;1: 1145.
30 Ashby M.F. Phil mag 1970;21: 399.
31 Fleck N.A., Muller G.M., Ashby M.F., Hutchinson J.W. Acta metall et mater 1994;42: 475.
32 Meyers M.A., Ashworth E. Phil mag 1982;46A: 737.
33 Benson D.J., Fu H-H., Meyers M.A. Mater sci eng 2001;A319–321: 854.
34 Carsley J.E., Milligan W.W., Zhu X.H., Aifantis E.C. Scripta mater 1997;36: 727.
35 Wei Q., Kecskes L., Jiao T., Hartwig K.T., Ramesh K.T., Ma E. Acta mater 2004; 52:1 959.
36 Nieh T.G., Wadsworth J. Scripta metall et mater 1991;25: 955.
37 Scattergood R.O., Koch C.C. Scripta metall et mater 1992;27: 1195.
38 Koch C.C. Nanostructured mater 1993;2: 109.
39 Pande C.S, Masumara R.A, Armstrong R.W. Nanostructured mater 1993;2: 323.
40 Gleiter H.. Progress in mater sci 1989;33: 223.
41 Thomas G.J., Siegel R.W., Eastman J.A. Scripta metall et mater 1990;24: 201.
42 Cheung C., Djuanda F., Erb U., Palumbo G. Nanostructured mater 1995;5: 513.
43 Lu K., Wei W.D., Wang J.T. Scripta metall et mater 1990;24: 2319.
44 Wang N., Wang Z., Aust K.T., Erb U. Mater sci eng 1997;A237: 150.
45 Xiao C., Mirshams R.A., Whang S.H., Yin W.M. Mater sci eng 2001;A301: 35.
46 Wang Y.M., Cheng S., Wei Q.M., Ma E., Nieh T.G., Hamza A. Scripta mater 2004;51: 1023.
47 Ebrahimi F., Bourne G.R., Kelly M.S., Matthews T.E. Nanostructured mater 1999;11: 343.
48 Agnew S.R., Elliott B.R., Youngdahl C.J., Hemker K.J., Weertman J.R. Mater sci eng 2000;A285: 391.
49 Weertman J.R. Mater sci eng 1993;A166: 161.
50 Sanders P.G., Fougere G.E., Thompson L.J., Eastman J.A., Weertman J.R. Nanostructured mater 1997;8: 243.
51 Sanders P.G., Witney A.B., Weertman J.R., Valiev R.Z., Siegel R.W. Mater sci eng 1995;A204: 7.
52 Gertsman V.Y., Birringer R. Scripta metall et mater 1994;30: 577.
53 Nabarro F.R.N. Report conf strength solids. The Physics Society. London. 1948; p.75.
54 Herring C. J appl phys 1950;21: 437.
55 Coble R.L. J appl phys 1963;34: 1679.
56 Gifkins R.C. J amer ceram soc 1968;51: 69.
57 Luthy H., White R.A, Sherby O.D. Mater sci eng 1979;39: 211.
58 Sanders P.G., Rittner M., Kiedaisch E., Weertman J.R., Kung H., Lu Y.C. Nanostructured mater 1997;9: 433.
59 Wang D.L., Kong Q.P., Shui J.P. Scripta metall et mater 1994;31: 47.
60 Deng J., Wang D.L., Kong Q.P., Shui J.P. Scripta metall et mater 1995;32: 349.
61 Kong Q.P., Cai B., Xiao M.L. Mater sci eng 1997;A234–236: 91.
62 Cai B., Kong Q.P., Lu L., Lu K. Scripta mater 1999;41: 755.

63 Jia D., Ramesh K.T., Ma E., Lu L., Lu K. Scripta mater 2001;45: 613.
64 Yin W.M., Whang S.H., Mirshams R., Xiao C.H. Mater sci eng 2001;A301: 18.
65 Wang Y.M., Hamza A.V., Ma E. Acta mater 2006;54: 2715.
66 Wang Y.M., Ma E. Appl phys letts 2004;85: 2750.
67 Vehoff H., Lemaire D., Schuler K., Waschkies T., Yang B. Int J mater res 2007;98: 259.
68 Kumar K.S., Suresh S., Chisholm M.F., Horton J.A., Wang P. Acta mater 2003;51: 387.
69 Chen M., Ma E., Hemker K.J., Sheng H., Wang Y., Cheng X. Science 2003;300: 1275.
70 Liao X.Z., Zhao Y.H., Srinivasan S.G., Zhu Y.T., Valiev R.Z., Gunderov D.V. Appl phys letts 2004;84: 592.
71 Zhu Y.T., Liao X.Z., Srinivasan S.G., Zhao Y.H., Baskes M.I., Zhou F., Lavernia E.J. Appl phys letts 2004;85: 5049.
72 Budrovic Z., Van Swygenhoven H., Derlet P.M., Van Petegem S., Schmitt B. Science 2004;304: 273.
73 Shan Z., Stach E.A., Wiezorek J.M.K., Knapp J.A., Follstaedt, Mao S.X. Science 2004;305: 654.
74 Asaro R.J., Krysl P., Kad B. Phil mag letts 2003;83: 733.
75 Cheng S., Spencer J.A., Milligan W.W. Acta mater 2003;51: 4505.
76 Schiotz J., Vegge T., Di Tolla F.D., Jacobsen K.W. Phys rev 1999;B60: 11,971.
77 Van Swygenhoven H., Caro A., Farkas D. Scripta mater 2001;44: 1513.
78 Derlet P.M., Hasnaoui A., Van Swygenhoven H. Scripta mater 2003;49: 629.
79 Van Swygenhoven H., Caro A. Phys rev 1998;B58: 11,246.
80 Van Swygenhoven H., Derlet P.M., Froseth A.G. Nature materials 2004;3: 399.
81 Schiotz J., Di Tolla F.D., Jacobsen K.W. Nature 1998;391: 561.
82 Schiotz J., Jacobsen K.W. Science 2003;301: 1357.
83 Van Vliet K.J., Tsikata S., Suresh S. Appl phys letts 2003;83: 1441.
84 Morris D.G., Morris M.A. Acta metall mater 1991;39: 1763.
85 Hansen N. Scripta mater 2004;51: 801.
86 Hansen N. Adv eng mater 2005;7: 815.
87 Morris-Muñoz M.A., Dodge A., Morris D.G. Nanostructured mater 1999;11: 873.
88 Morris D.G., Gutierrez-Urrutia I., Muñoz-Morris M.A. Scripta mater 2007;57: 369.
89 Krasnowski M., Witek A., Kulik T. Intermetallics 2002;10: 371.
90 Krasnowski M., Kulik T. Intermetallics 2007;15: 201.
91 Krasnowski M., Kulik T. Intermetallics 2007;15: 1377.
92 He L., Ma E. Nanostructured mater 1996;7: 327.
93 Botcharova E., Freudenberger J., Schultz L. Acta mater 2006;54: 3333.
94 Venugopal T., Prasad Rao K., Murty B.S. Acta mater 2007;55: 4439.
95 Dutta A., De P.S., Mishra R.S., Watson T.J. Mater sci eng 2009;A513–514: 239.
96 Koch C.C. Scripta mater 2003;49: 657.
97 Benameur T., Yavari A.R. J mater res 1992;7: 2971.
98 Morris D.G., Amils X., Nogues J., Surinach S., Baro M.D., Muñoz-Morris M.A. Int J of non-equilib proc 2002;11: 379.
99 Lu L., Shen Y.F., Chen X.H., Qian L.H., Lu K. Science 2004;304: 422.
100 Li Y.S., Tao N.R., Lu K. Acta mater 2008;56: 230.
101 Zhang Y., Tao N.R., Lu K. Acta mater 2008;56: 2429.
102 Tao N.R., Lu K. J mater sci technol 2007;23: 771.
103 Qin E.W., Lu L., Tao N.R., Tan J., Lu K. Acta mater 2009;57: 6215.
104 Christian J.W., Mahajan S. Prog mater sci 1995;39: 1.
105 Valiev R.Z., Islamgaliev R.K., Alexandrov I.V. Progress in mater sci 2000;45: 103.

106 Valiev R.Z., Langdon T.G. Progress in mater sci 2006;51: 881.
107 Cabibbo M., Evangelista E., Kassner M.E., Meyers M.A. Microstructure and strength of metals processed by severe plastic deformation. In: Zhu Y.T., Langdon T.G., Horita Z., Zehetbauer M.J., Semiatin S.L., Lowe T.C., editors. Ultrafine Grained Materials IV, TMS, Warrendale, 2006; p.237.
108 Gubicza J., Chinh N.Q., Langdon T.G., Ungar T. Microstructure and strength of metals processed by severe plastic deformation. In: Zhu Y.T., Langdon T.G., Horita Z., Zehetbauer M.J., Semiatin S.L., Lowe T.C., editors. Ultrafine Grained Materials IV, TMS, Warrendale, 2006; p.231.
109 Valiev R.Z., Ivanisenko Y.V., Rauch E.F., Baudelet B. Acta mater 1996;44: 4705.
110 Morris D.G., Gutierrez-Urrutia I., Muñoz-Morris M.A. J mater sci 2008;43: 7438.
111 Leseur D.R., Syn C.K., Sherby O.D. Mater sci eng 2007;A463: 54.
112 Morris D.G., Gutierrez-Urrutia I., Muñoz-Morris M.A., to be published.
113 Fecht H.J. Formation of Nanostructures in Metals and Composites by Mechanical Means. In: Zehetbauer M.J., Valiev R.Z., editors. Nanomaterials by Severe Plastic Deformation, Wiley-VCH, Weinheim, 2004; p.30.
114 Todaka Y., Umemoto M., Yin J., Liu Z., Tsuchiya K. Mater sci eng. 2007;A462: 264.
115 Zadra M., Casari F., Lonardelli I., Ischia G., Molinari A. Intermetallics 2007;15: 1650.